

## Polymeric Luminescent Zn(II) and Cd(II) Dicarboxylates Decorated by Oxime Ligands: Tuning the Dimensionality and Adsorption Capacity

Published as part of the Crystal Growth & Design Mikhail Antipin Memorial virtual special issue

Lilia Croitor,<sup>§</sup> Eduard B. Coropceanu,<sup>†</sup> Artém E. Masunov,<sup>‡,§</sup> Hector J. Rivera-Jacquez,<sup>‡</sup> Anatolii V. Siminel,<sup>§</sup> Vyacheslav I. Zelentsov,<sup>§</sup> Tatiana Ya. Datsko,<sup>§</sup> and Marina S. Fonari\*,<sup>§</sup>

<sup>§</sup>Institute of Applied Physics Academy of Sciences of Moldova, Academy str., 5 MD2028, Chisinau, Moldova

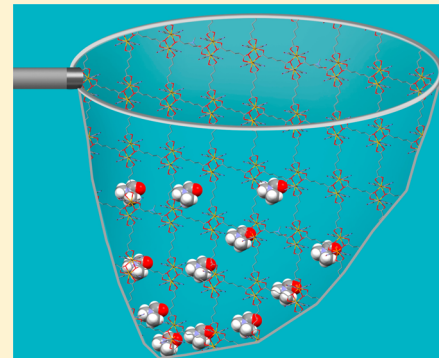
<sup>†</sup>Institute of Chemistry Academy of Sciences of Moldova, Academy str., 3 MD2028, Chisinau, Moldova

<sup>‡</sup>NanoScience Technology Center, and Department of Chemistry, University of Central Florida, Orlando, Florida 32826, United States

<sup>#</sup>Department of Physics, and Florida Solar Energy Center, University of Central Florida, Orlando, Florida 32826, United States

### Supporting Information

**ABSTRACT:** Ten Zn(II) and Cd(II) metal–organic materials were synthesized and studied by the X-ray method. Among these 10 structures, two represent binuclear clusters, and two are one-dimensional (1D) coordination polymers, while five are laminar two-dimensional (2D) solids and one is the three-dimensional (3D) framework. The investigation has been aimed at rational design of coordination polymers decorated by oxime ligands to increase the accessible adsorption area in these newly synthesized solids. The ligands used include three aliphatic dicarboxylic acids, HOOC-(CH<sub>2</sub>)<sub>n</sub>-COOH [n = 1, 2, 4 corresponding to malonic (H<sub>2</sub>mal), succinic (H<sub>2</sub>suc), and adipic (H<sub>2</sub>adi) acids], and three neutral oxime ligands [pyridine-2-aldoxime (2-pyao), pyridine-4-aldoxime (4-pyao), and 1,2-cyclohexanedionedioxime (Niox)]. These novel hybrid solids with the compositions [Zn<sub>2</sub>(suc)<sub>2</sub>(2-pyao)<sub>4</sub>]·2H<sub>2</sub>O **1**, [Cd<sub>2</sub>(suc)<sub>2</sub>(2-pyao)<sub>4</sub>(H<sub>2</sub>O)<sub>2</sub>][BF<sub>4</sub>]<sub>2</sub> **2**, [Cd(suc)<sub>2</sub>(2-pyao)<sub>2</sub>]<sub>n</sub> **3**, [Zn(mal)(4-pyao)(H<sub>2</sub>O)]<sub>n</sub> **4**, [Cd(mal)(4-pyao)(H<sub>2</sub>O)]<sub>n</sub> **5**, [Zn(suc)(4-pyao)]<sub>n</sub> **6**, [Zn(adi)(4-pyao)<sub>2</sub>]<sub>n</sub> **7**, {[Cd(adi)(4-pyao)<sub>2</sub>]·dmf}<sub>n</sub> **8**, [Zn(adi)(Niox)]<sub>n</sub> **9**, and [Cd(adi)(Niox)]<sub>n</sub> **10** [dmf – N,N'-dimethylformamide] demonstrate a variable class of coordination supramolecular architectures dictated by the distinctions in the metals' and oxime ligands' coordination capacities and preferences, and length and flexibility of the dicarboxylic linkers. The discrete aggregates **1** and **2** differ by the components' ratio and conformation of the bridging succinate anion; compounds **3** and **7** are 1D arrays, and compounds **4**, **5**, **6**, **8**, and **9** represent 2D layers of different topologies. Compound **10** is a 3D grid afforded by the concerted contribution of the longest in this series adipate anion, and the bigger atomic radius Cd(II) vs. Zn(II). The adsorptive properties of **7** and **9** are reported. For the laminar solid **9**, the quantum chemical simulations of the adsorption capacity are in line with the experimental results. All new materials reveal dual green-blue wavelength emission in the solid state.



### INTRODUCTION

Since the seminal works by Yaghi et al.,<sup>1</sup> Zn(II) and Cd(II) metal–organic frameworks (MOF)<sup>1–7</sup> and metal organic materials (MOM)<sup>8</sup> in general continue to attract close attention of the scientific community interested in new materials with fascinating adsorptive,<sup>1–12</sup> catalytic,<sup>13–18</sup> and sensor properties.<sup>19</sup> For these particular coordination networks, the high adsorption capacities,<sup>1–12</sup> luminescent,<sup>20–23</sup> and nonlinear optical (NLO)<sup>24–29</sup> properties should be mentioned first. The NLO properties of MOMs are being investigated in relation to several technological applications, including optical communications and upconversion lazing.<sup>27</sup> The third-order nonlinearities, such as two-photon absorption (2PA), present special interest, as they are not limited to noncentrosymmetric structures,<sup>30</sup> unlike the second-order nonlinearities.<sup>31,32</sup> Several recent studies indicated

that 2PA properties are enhanced by metal coordination compared to free ligands.<sup>28,29</sup> We recently explained this enhancement using approximate second-order density functional theory.<sup>33,34</sup> From the crystal engineering viewpoint, Zn(II) and Cd(II) ions have the same d<sup>10</sup> electronic configuration, yet they are dissimilar in their atomic radii and coordination capacities. This could justify the huge number of the homoligand, primarily carboxylate and mixed-ligand, primarily carboxylate-aromatic amine-based coordination networks including both isostructural and isomorphous analogues, and the supramolecular isomers as well.<sup>35–39</sup> The experimental efforts aimed at the forthcoming

**Received:** April 18, 2014

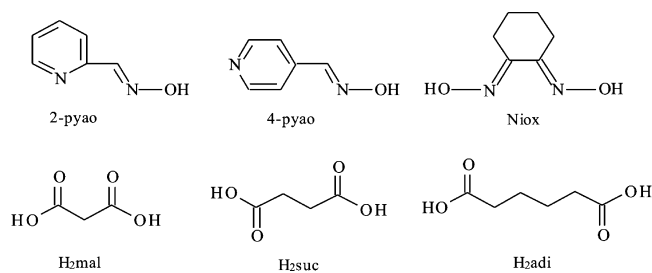
**Revised:** June 22, 2014

**Published:** July 23, 2014

MOF materials with large pores, efficient guest uptake, and stability<sup>40,41</sup> continue. Theoretical studies complement experiment by predicting adsorption capacity, adsorption preference, and desired optical properties of MOMs including the Zn(II)/Cd(II)-based ones.<sup>42–45</sup> In our previous reports, we used the mixed-ligand “blend approach”<sup>46,47</sup> for decoration of coordination polymers (CP) by oxime ligands.<sup>48–53</sup> We concluded that the coordination of bulky neutral oxime ligands to the d<sup>10</sup> metals provides the loosely packed MOMs with the voids in the crystal lattice for inclusion of small guest molecules, such as water and dmfs. Our studies undertaken so far revealed that the oxime molecules coordinated as the terminal ligands impose restrictions on the dimensionality of coordination networks. Those one- and two-dimensional (1D and 2D) polymeric materials were capable of holding the guest molecules in their voids. While some of them held their coordination frameworks in the guest-free state spontaneously or after evacuation of the adsorbed dmfs guest molecules (resulting in the crystal-to-crystal transformation in the solid state), the others failed.<sup>51,53</sup> The quantum-chemical calculations undertaken by us convincingly confirmed the dual luminescence and the LLCT emission mechanism in the 2-pyao containing MOMs.<sup>53</sup> Our very recent study based on a series of 4-pyao containing 1D Zn(II)/Cd(II) supramolecular isomers suggests several guidelines for the rational design of acentric polymeric materials for NLO applications.<sup>33</sup>

In order to search for the new coordination networks herein, we have combined the Zn(II)/Cd(II) metal centers with two types of ligands, flexible aliphatic dicarboxylic acids of different length, HOOC-(CH<sub>2</sub>)<sub>n</sub>-COOH ( $n = 1, 2, 4$ ) including malonic (H<sub>2</sub>mal), succinic (H<sub>2</sub>suc), and adipic acids (H<sub>2</sub>adi), and three oxime ligands, including pyridine-2-aldoxime (2-pyao), pyridine-4-aldoxime (4-pyao), and 1,2-cyclohexanedionedioxime (Niox). The ligands used in this study are shown in Scheme 1.

**Scheme 1. Structural Formulae for Ligands with Acronyms Used in This Study**



The preliminary CSD search [CSD version 5.35, update February 2014] along with a literature review<sup>54–57</sup> revealed that the chosen aliphatic dicarboxylic acids can coordinate simultaneously from one up to six Zn(II)/Cd(II) metal centers (Figure 1S in Supporting Information), thus providing possibilities for polymeric coordination networks. This contribution represents an effort to rationalize the dimensionality of coordination networks including the dicarboxylic acids and the oxime ligands. Ten Zn(II) and Cd(II) MOMs with the compositions [Zn<sub>2</sub>(suc)<sub>2</sub>(2-pyao)<sub>4</sub>]·2H<sub>2</sub>O **1**, [Cd<sub>2</sub>(suc)(2-pyao)<sub>4</sub>(H<sub>2</sub>O)<sub>2</sub>]·[BF<sub>4</sub>]<sub>2</sub> **2**, [Cd(suc)(2-pyao)<sub>2</sub>]<sub>n</sub> **3**, [Zn(mal)(4-pyao)(H<sub>2</sub>O)]<sub>n</sub> **4**, [Cd(mal)-(4-pyao)(H<sub>2</sub>O)]<sub>n</sub> **5**, [Zn(suc)(4-pyao)]<sub>n</sub> **6**, [Zn(adi)(4-pyao)<sub>2</sub>]<sub>n</sub> **7**, {[Cd(adi)(4-pyao)<sub>2</sub>]·dmf}<sub>n</sub> **8**, [Zn(adi)(Niox)]<sub>n</sub> **9**, and [Cd(adi)(Niox)]<sub>n</sub> **10** were synthesized and studied by the

X-ray method. These novel metal–organic solids demonstrate both similarities and dissimilarities in coordination supramolecular architectures dictated by the distinctions in the coordination capacity of the metals and oxime ligands, as well as in the length and flexibility of the dicarboxylic spacers.

## EXPERIMENTAL SECTION

**Materials and General Procedures.** WARNING: Cadmium salts are carcinogenic and toxic.<sup>58</sup> All reagents and solvents were obtained from commercial sources and were used without further purification. Elemental analyses were performed on an Elementar Analysensysteme GmbH Vario El III elemental analyzer. The IR spectra were obtained in Nujol on a FT IR Spectrum-100 PerkinElmer spectrometer in the range of 400–4000 cm<sup>-1</sup>. Emission spectra were measured for monocrystals at room temperature on an Excitation YAG:Nd3+ laser, third harmonic generation,  $\lambda = 355$  nm, duration =10 ns, time repetition 10 Hz. The nitrogen adsorption–desorption isotherms have been measured using an ASAP2000 micrometer device. All the solids were obtained by the same solvent crystallization techniques using the mixing of warm solutions of starting components and simultaneous cooling of final solutions. The details of the synthetic procedures together with the data of the elemental analyses and IR spectra are given in Supporting Information.

**Crystallographic Studies.** The X-ray data for **1–10** were collected at room temperature on an Oxford Diffraction Xcalibur diffractometer equipped with CCD area detector and a graphite monochromator utilizing Mo K $\alpha$  radiation. Final unit cell dimensions were obtained and refined on an entire data set. All calculations to solve the structures and to refine the model proposed were carried out with the programs SHELXS97 and SHELXL97.<sup>59</sup> In all structures, the C-bounded H atoms were placed in calculated positions and were treated using a riding model approximation with  $U_{\text{iso}}(\text{H}) = 1.2U_{\text{eq}}(\text{C})$ ; the O-bounded H-atoms were found from differential Fourier maps at the intermediate stages of the refinement, and their positions were constrained using the AFIX 83 instruction in SHELXL for oxime groups, while the O–H and H···H distances were restrained as 0.86(1) and 1.46(1) Å in the water molecules in **1**, **2**, and **5**. These hydrogen atoms were refined with isotropic displacement parameter  $U_{\text{iso}}(\text{H}) = 1.5U_{\text{eq}}(\text{O})$ . The [BF<sub>4</sub>]<sup>-</sup> anion in **2** is disordered over two positions with the partial occupancies 0.741(5) and 0.259(5). Its regular tetrahedral geometry was modeled using geometric restraints imposed for B–F bond distances and F···F interatomic distances to keep them equal. Both disordered positions were refined in anisotropic approximation with the equal anisotropic displacement parameters for the similar atoms. In **8** the dmfs molecule is disordered over two positions around an inversion center with the partial occupancies 0.711(5) and 0.289(5), and the pyridine ring of one of the 4-pyao molecules is disordered over two positions with the partial occupancies 0.67(3) and 0.33(3). The disordered fragments were refined in anisotropic approximation using equal anisotropic displacement parameters for the similar atoms. The X-ray data and the details of the refinement for **1–10** are summarized in Table 1. The figures were produced using Mercury.<sup>60</sup> Solvent accessible voids (SAVs) and Kitagorodskii’s Packing Index (PI) were calculated using PLATON.<sup>61</sup>

## RESULTS AND DISCUSSION

**General.** The reaction blend was modified by excluding the bipyridine ligands from the “mixed ligand blend”.<sup>48–52</sup> This was done in order to promote the reaction to favor oxime ligands since they compete with the bipyridine in the coronation of the metal centers. Furthermore, in order to avoid competition with the starting acetate anion, the Zn(II)/Cd(II) tetrafluoroborate salts were also used in this study keeping in mind the tetrafluoroborate anion good-leaving properties. The use of the trade starting materials rationalizes the low-cost synthetic procedures and might be considered as an advantage of this research. The IR spectra confirm the presence of organic ligands used in the syntheses through the typical vibrations of the

Table 1. Crystallographic Data and Structure Refinement Details for Compounds 1–10

	1	2	3	4	5
empirical formula	C <sub>32</sub> H <sub>36</sub> N <sub>8</sub> O <sub>14</sub> Zn <sub>2</sub>	C <sub>28</sub> H <sub>32</sub> B <sub>2</sub> F <sub>8</sub> N <sub>8</sub> O <sub>10</sub> Cd <sub>2</sub>	C <sub>16</sub> H <sub>16</sub> N <sub>4</sub> O <sub>6</sub> Cd	C <sub>9</sub> H <sub>10</sub> N <sub>2</sub> O <sub>6</sub> Zn	C <sub>9</sub> H <sub>10</sub> N <sub>2</sub> O <sub>6</sub> Cd
formula weight	887.43	1039.04	472.73	307.56	354.59
crystal system	triclinic	triclinic	monoclinic	orthorhombic	orthorhombic
space group	P <bar{1}< td=""><td>P<bar{1}< td=""><td>P<sub>2</sub><sub>1</sub>/n</td><td>Pnma</td><td>Aba2</td></bar{1}<></td></bar{1}<>	P <bar{1}< td=""><td>P<sub>2</sub><sub>1</sub>/n</td><td>Pnma</td><td>Aba2</td></bar{1}<>	P <sub>2</sub> <sub>1</sub> /n	Pnma	Aba2
Z	1	1	4	4	8
a (Å)	9.5986(7)	8.0455(7)	10.5244(3)	22.3659(10)	21.9763(10)
b (Å)	9.6754(7)	11.0296(9)	15.4351(3)	7.2649(5)	10.4278(4)
c (Å)	10.1798(7)	12.2367(9)	10.9498(3)	7.2828(3)	10.7628(4)
α (deg)	79.665(6)	81.545(7)	90	90	90
β (deg)	82.116(6)	72.039(7)	91.508(2)	90	90
γ (deg)	87.581(6)	69.327(8)	90	90	90
V (Å <sup>3</sup> )	921.12(11)	965.55(14)	1778.13(8)	1183.35(11)	2466.45(17)
D <sub>c</sub> (g/cm <sup>-3</sup> )	1.600	1.787	1.766	1.726	1.910
μ (mm <sup>-1</sup> )	1.381	1.202	1.270	2.097	1.792
F(000)	456	514	944	624	1392
reflns collected/unique	4892/2762	3309/2346	6539/2583	3272/1021	4426/1627
reflns with [I > 2σ(I)]	3570	2756	3125	1132	1981
data/restraints/params	3570/3/261	2756/41/281	3125/0/248	1132/0/100	1981/4/169
GOF on F <sup>2</sup>	0.999	1.047	0.997	1.000	0.998
R <sub>1</sub> , wR <sub>2</sub> [I > 2σ(I)]	0.0464, 0.0836	0.0411, 0.0872	0.0308, 0.0715	0.0299, 0.0812	0.0376, 0.0593
R <sub>1</sub> , wR <sub>2</sub> (all data)	0.0671, 0.0956	0.0502, 0.0960	0.0410, 0.0778	0.0341, 0.0843	0.0533, 0.0650
	6	6a	7	8	9
empirical formula	C <sub>10</sub> H <sub>10</sub> N <sub>2</sub> O <sub>5</sub> Zn	C <sub>16</sub> H <sub>18</sub> N <sub>4</sub> O <sub>6</sub>	C <sub>18</sub> H <sub>20</sub> N <sub>4</sub> O <sub>6</sub> Zn	C <sub>21</sub> H <sub>27</sub> N <sub>5</sub> O <sub>7</sub> Cd	C <sub>12</sub> H <sub>18</sub> N <sub>2</sub> O <sub>6</sub> Zn
formula weight	303.57	362.34	453.75	573.88	351.65
crystal system	monoclinic	monoclinic	triclinic	triclinic	monoclinic
space group	P <sub>2</sub> <sub>1</sub> /c	C2/c	P <bar{1}< td=""><td>P<bar{1}< td=""><td>P<sub>2</sub><sub>1</sub>/c</td></bar{1}<></td></bar{1}<>	P <bar{1}< td=""><td>P<sub>2</sub><sub>1</sub>/c</td></bar{1}<>	P <sub>2</sub> <sub>1</sub> /c
Z	4	4	2	2	4
a (Å)	14.6217(3)	21.078(3)	8.2196(6)	9.9339(5)	10.2393(5)
b (Å)	8.5579(2)	4.7782(4)	9.2915(5)	10.8715(8)	15.3424(7)
c (Å)	9.3563(2)	18.462(2)	14.0247(8)	13.3713(9)	9.6520(5)
α (deg)	90	90	77.376(5)	66.832(7)	90
β (deg)	93.319(2)	114.867(14)	84.259(5)	86.057(5)	105.727(5)
γ (deg)	90	90	75.489(5)	73.598(5)	90
V (Å <sup>3</sup> )	1168.80(4)	1687.1(3)	1010.70(11)	1272.10(14)	1459.52(12)
D <sub>c</sub> (g/cm <sup>-3</sup> )	1.725	1.427	1.491	1.498	1.600
μ (mm <sup>-1</sup> )	2.116	0.111	1.257	0.906	1.711
F(000)	616	760	468	584	728
reflns collected/unique	3656/1745	2595/1643	5767/3141	8267/3993	4689/1655
reflns with [I > 2σ(I)]	2038	1154	3930	4465	2571
data/restraints/params	2038/0/163	1643/1/122	3930/0/262	4465/9/334	2571/1/207
GOF on F <sup>2</sup>	1.000	1.085	1.000	0.999	0.999
R <sub>1</sub> , wR <sub>2</sub> [I > 2σ(I)]	0.0406, 0.1043	0.0543, 0.1195	0.0423, 0.0860	0.0354, 0.0923	0.0562, 0.1020
R <sub>1</sub> , wR <sub>2</sub> (all data)	0.0489, 0.1116	0.0812, 0.1446	0.0569, 0.0934	0.0416, 0.0972	0.0989, 0.1193
	10				

oxime group and/or pyridine aromatic rings, and carboxylic groups. The presence of oxime ligands was documented by the oscillations  $\nu(\text{C}=\text{N})$  at  $\sim 1600 \text{ cm}^{-1}$ ,  $\nu_{\text{asym}}(\text{N}-\text{O})$  at  $12228\text{--}1221 \text{ cm}^{-1}$ , and  $\nu_{\text{symm}}(\text{N}-\text{O})$  at  $1110\text{--}1050 \text{ cm}^{-1}$ . The presence of carboxylate ligand was fixed by the  $\nu_{\text{as}}$  (OCO) and  $\nu_{\text{s}}$  (OCO) absorption bands that appeared in the ranges  $1582\text{--}1550$  and  $1480\text{--}1430 \text{ cm}^{-1}$ , respectively, whereas the  $\delta(\text{OCO})$  absorptions were located nearby  $825$  and  $740 \text{ cm}^{-1}$ . The asymmetric and symmetric stretching vibrations of the CH<sub>2</sub> groups were fixed by the bands in the  $2980\text{--}2922$  and  $2890\text{--}2623 \text{ cm}^{-1}$  regions (see Supporting Information for details).<sup>62</sup>

**Crystal Structures.** MOMs from the system Zn(II)/Cd(II)-2-pyao-H<sub>2</sub>suc include two discrete binuclear complexes, [Zn<sub>2</sub>(suc)<sub>2</sub>(2-pyao)<sub>4</sub>] $\cdot$ 2H<sub>2</sub>O **1** (Figure 1), [Cd<sub>2</sub>(suc)(2-pyao)<sub>4</sub>(H<sub>2</sub>O)<sub>2</sub>][BF<sub>4</sub>]<sub>2</sub> **2** (Figure 2), and 1D coordination polymer [Cd(suc)(2-pyao)<sub>2</sub>]<sub>n</sub> **3** (Figure 3). Compound **1** represents

the neutral binuclear molecule, the ionic compound **2** is built of the binuclear cations, [Cd<sub>2</sub>(suc)(2-pyao)<sub>4</sub>] $\cdot$ 2H<sub>2</sub>O<sup>2+</sup> and [BF<sub>4</sub>]<sup>-</sup> anions held together via OH $\cdots$ F hydrogen bonds, and compound **3** is the neutral 1D polymer. In all three solids, the metal: 2-pyao molar ratio is 1:2, and the metal coordination cores are the distorted N<sub>4</sub>O<sub>2</sub> octahedra that comprise the two 2-pyao ligands coordinated via pyridine and oxime N-binding sites, two succinate anions in **1** and **3**, and one succinate anion and one water molecule in **2**. In all cases, the terminal 2-pyao ligands take the common bidentate chelating coordination mode that results in the five-membered chelate rings with the Zn–N distances being in the range of  $2.151(3)\text{--}2.283(3) \text{ \AA}$ , and the Cd–N distances being in the range of  $2.323(4)\text{--}2.376(4) \text{ \AA}$  (Table 1S, Supporting Information). The two 2-pyao ligands display in nearly perpendicular planes as the dihedral angles between their five-membered metallocycles of  $89.1^\circ$  in **1**,  $79.35^\circ$  in **2**, and

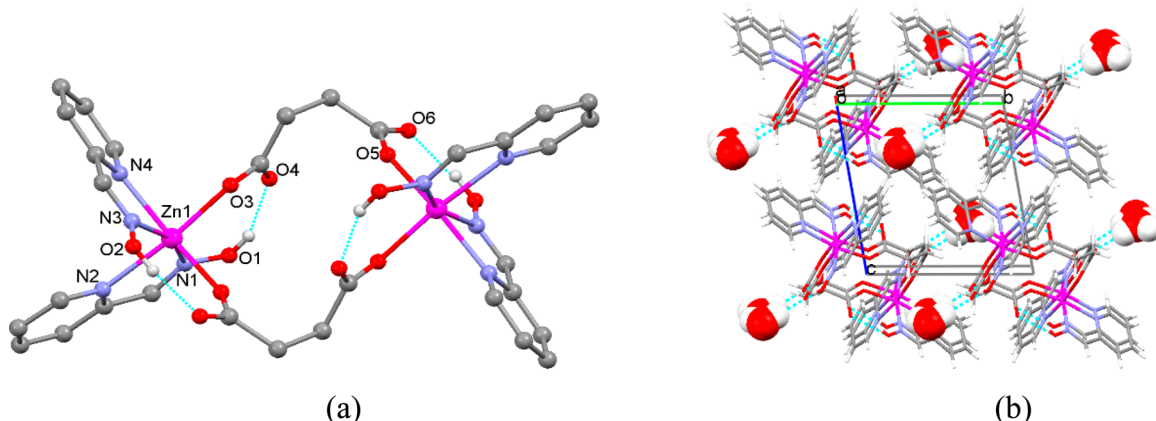


**Figure 1.** (a) View of the binuclear complex  $[\text{Zn}_2(\text{suc})_2(2\text{-pyao})_4]$  in **1** with the partial numbering scheme. C-bound H atoms are omitted for clarity. (b) The fragment of crystal packing with water molecules inclusion. Water molecules are shown in space-filling mode.

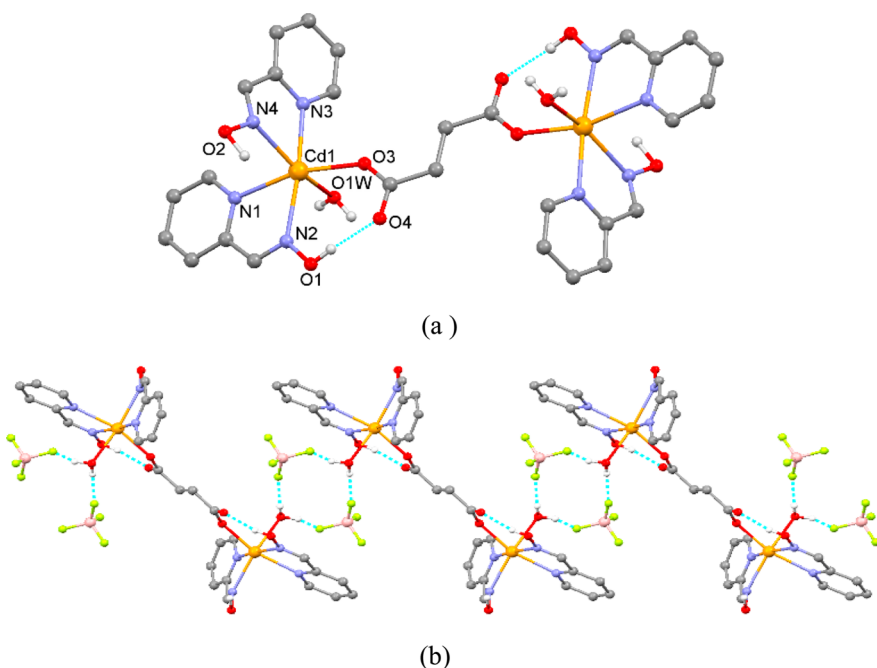


**Figure 2.** (a) View of the binuclear cation  $[\text{Cd}_2(\text{suc})(2\text{-pyao})_4(\text{H}_2\text{O})_2]^{2+}$  in **2** with the partial numbering scheme. C-bound H atoms are omitted for clarity. (b) The fragment of 1D chain in **2** sustained by  $\text{OH}\cdots\text{F}$  hydrogen bonds.

71.60° in **3** indicate. The succinate linkers coordinate to the metals in the monodentate bridging modes in **1** and **2**, and in monodentate and bidentate bridging modes in **3** (Scheme 1S, Supporting Information). In compounds **1** and **2**, the second oxygen of the carboxylic group is fixed by its involvement in the intramolecular  $\text{OH}\cdots\text{O}$  hydrogen bond with the oxime hydroxyl group (Table 2S, Supporting Information). The anion's conformation changes substantially from the twisted *gauche* to the extended *trans* one, as it is obvious from the  $\text{C}-\text{C}-\text{C}-\text{C}$  torsion angle being 68.76° in **1**, 180° in **2**, and 176.1° in **3**. This is also reflected in the scattering of the metal···metal separations across the succinate anion, being 6.780 Å in **1**, 9.207 Å in **2**, and 9.774 Å in **3**. The flexibility of succinate anion in coordination networks has been documented.<sup>63–70</sup> The  $\text{Zn}\cdots\text{Zn}$  separation of 6.780 Å in **1** is longer compared with 4.999 Å in the recently reported by us binuclear cluster  $[(\text{ZnSO}_4)_2(2\text{-pyao})_4]\cdot\text{dmf}\cdot 2\text{H}_2\text{O}$ <sup>53</sup> with two sulfate anions as the bridging ligands. The extended conformation of succinate anion in Cd(II) MOM **2**,

MOM **3**, and in the reported examples supports structure **1** with possible extension of up to at least 1D polymer analogous to **3**. The ionic compound **2** could be considered as the precursor for **3**, most probably capable of being transformed to the latter one through the simultaneous removal of water molecule from the metal coordination core and  $[\text{BF}_4]^-$  anions from the second coordination sphere. The isolation of **3** as an individual compound supports this suggestion. The hydrophilic regions adsorb water molecules in **1** and  $[\text{BF}_4]^-$  anions in **2**, and these species are held in the crystal lattices via  $\text{OH}\cdots\text{O}$  and  $\text{OH}\cdots\text{F}$  hydrogen bonds (Figure 1b, Figure 2b, Table 2S). The guest-free 1D coordination polymer **3** packs in a zipper-like mode with the intercalation of tapes providing the interpenetration of the tapes accompanied by the parallel arrangement of the aromatic fragments (Figure 3b). The crystal structure organization in **3** is very close to the series of 1D coordination polymers with the general formula  $\{[\text{M}(\text{bdc})(2\text{-pyao})]\cdot\text{dmf}\}_n$  ( $\text{M} = \text{Mn}(\text{II}), \text{Zn}(\text{II}), \text{Cd}(\text{II})$ ;  $\text{bdc} = 1,4\text{-benzenedicarboxylate acid}$ ) hosted dmf

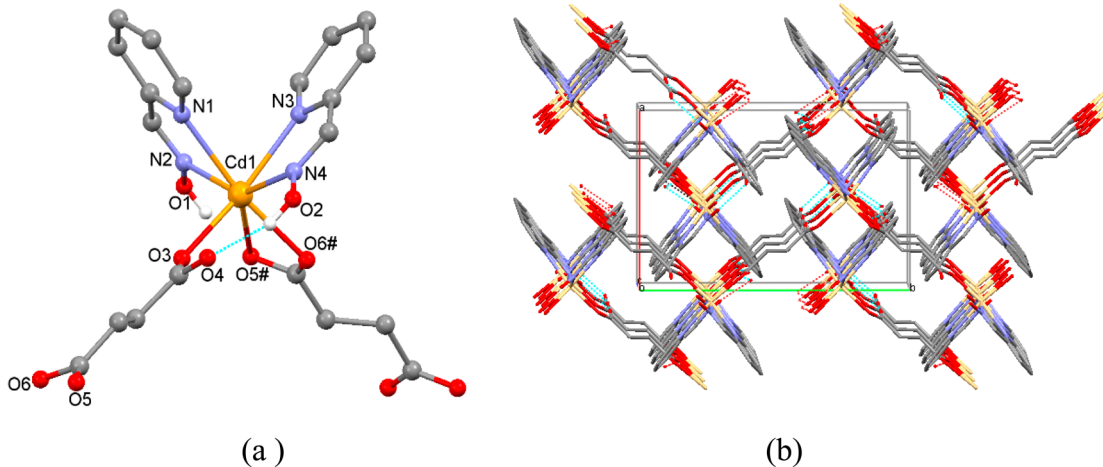


**Figure 3.** (a) View of the metal building unit (MBU) in 3 with partial numbering scheme. Symmetry transformation for the symmetry-related atoms: #  $\frac{1}{2} - x, y - \frac{1}{2}, z$ . (b) Packing of the interdigitated 1D tapes in 3. H atoms are omitted for clarity.

solvent,<sup>53</sup> and thus similarly might potentially include small guest molecules (dmf for example) in the rectangular compartments of the pseudo 3D grid.

We conclude this section by noting that the currently known examples demonstrate the possibility of exclusively 1D coordination polymers via the combination of Zn(II)/Cd(II)-2-pyao unit with dicarboxylate linkers that is justified by the coordination preferences of the 2-pyao ligand.

MOMs from the system Zn(II)/Cd(II)-4-pyao-dicarboxylic acid ( $H_2\text{mal}$ ,  $H_2\text{suc}$ ,  $H_2\text{adi}$ ) include five coordination polymers,  $[\text{Zn}(\text{mal})(4\text{-pyao})(\text{H}_2\text{O})]_n$  **4**,  $[\text{Cd}(\text{mal})(4\text{-pyao})(\text{H}_2\text{O})]_n$  **5**,  $[\text{Zn}(\text{suc})(4\text{-pyao})]_n$  **6**,  $[\text{Zn}(\text{adi})(4\text{-pyao})]_n$  **7**, and  $\{[\text{Cd}(4\text{-pyao})_2(\text{adi})_2]\cdot\text{dmf}\}_n$  **8**, four of which, **4**, **5**, **6**, and **8**, represent the 2D laminar structures, and one, **7**, represents the 1D coordination polymer. The metal/oxime molar ratio is 1:1 in **4–6**, and 1:2 in **7** and **8**. In all compounds the 4-pyao ligand coordinates in a monodentate mode via pyridine nitrogen atom and occupies one or two coordination places in the MBU.

The two 2D coordination polymers **4** and **5** with the same composition,  $[\text{M}(\text{mal})(4\text{-pyao})(\text{H}_2\text{O})]_n$  [ $\text{M} = \text{Zn(II)}, \text{Cd(II)}$ ], represent the supramolecular isomers<sup>35</sup> that crystallize in the orthorhombic centrosymmetric space group *Pnma* (**4**), and acentric space group *Aba2* (**5**). The Zn(II) atom locates on the mirror plane in **4**, while Cd(II) atom—in general position in **5**. Both metal atoms adjust the slightly distorted  $\text{N}_1\text{O}_5$ -octahedral cores (Figure 4a,b) provided by three identical malonate anions acting in bidentate-chelating and monodentate bridging modes each in the equatorial plane, the distances Zn—O 2.0778(17)–2.0853(17) Å, the distances Cd—O 2.285(5)–2.343(5) Å, and with the 4-pyao and water neutral molecules that occupy two axial positions, Zn—O( $\text{H}_2\text{O}$ ) 2.243(3), Zn—N 2.124(3) Å in **4**, and Cd—O( $\text{H}_2\text{O}$ ) 2.308(6), Cd—N 2.310(6) Å in **5**. Our survey of CSD revealed that this mode of malonate anion coordination is among the four common ones registered for this linker in the coordination networks (Scheme 1S, Supporting Information). The malonate anions are responsible for the similar 2D dense coordination networks with the (4,3) topology and the rhombohedral meshes (Figure 4c,d) with the linear dimensions of  $5.369 \times 5.369$  Å in **4**, and  $5.497 \times 5.656$  Å in **5** (measured as the metal···metal separations across the malonate ligands). The water molecules coordinated to the metals close these meshes via a couple of OH···O hydrogen bonds (Table 2S). In both crystals the layers propagate parallel to the *bc* crystallographic plane,

while the terminal pillar 4-pyao ligands are upright to these networks (Figure 4e, f). The layer thickness is 16.891 Å in **4** and 15.049 Å in **5**. The separations between the adjacent 4-pyao molecules attached to the metal cores in the layers equal to  $b = 7.26$  Å in **4** and  $1/2b = 5.21$  Å in **5** are appropriate for the interpenetration of the 4-pyao ligands from two adjacent layers. The interpenetrated layers are reinforced via OH(4-pyao)···O(1W) hydrogen bonds (Table 2S). The depth of layers' interdigitation is about 5.7 Å or ~30% of the layer's thickness in **4**, and of 4.1 Å or ~25% of the layer's thickness in **5**. Curiously the degree of interpenetration contradicts the available SAVs in these structures estimated by PLATON as 5.6% (PI 69.3) in **4** and 4.6% (PI 70.3) in **5**. Thus, having all the other parameters equal, the larger atomic radius of Cd(II) affords the higher conformational freedom for malonate anions and 4-pyao ligand thus providing the more effective crystal packing in comparison with the Zn(II) analogue **4**. These laminar solids can be considered as prospective adsorptive materials since: (a) the pillared 4-pyao ligands essentially increase their surface areas; (b) the structures contain hydrophilic and hydrophobic regions which might facilitate both protic and aprotic molecules inclusion; (c) the apohost<sup>71</sup> water molecules can be substituted by other neutral guests in the neutral-molecule exchange or by anionic linkers with the potential generation of 3D polymeric networks.

The combination of Zn(II)/Cd(II) salts with 4-pyao and succinic acid resulted in the 2D coordination polymer  $[\text{Zn}(4\text{-pyao})(\text{suc})_3]_n$  **6** and the organic salt (4-pyao-H)<sub>2</sub>(suc) **6a** as a byproduct. So far we were unable to obtain the Cd(II) analogues for this system. In the laminar structure **6**, the tetrahedral  $\text{NO}_3^-$  metal coordination core is originated from three crystallographically identical succinate anions and one 4-pyao neutral ligand (Figure 5a). The Zn—O bond distances in the coordination tetrahedron are in the range 1.916(3)–1.984(2) Å, and the Zn(1)–N(1) bond distance is equal to 2.053(2) Å. The layer with the (4,3) topology is provided by the mono, bidentate bridging succinate anions and is built of alternating 14- and 28-membered metallo rings (Figure 5b). The Zn···Zn separation across the carboxylic group is 5.035 Å, across the succinate ligand in the smaller ring is 5.44 Å, and across the bigger one is 7.84 Å. The layer thickness is equal to 21.461 Å. Similar to **4** and **5**, the interpenetration of the layers is observed (Figure 5c). The depth of interpenetration is 6.86 Å or ~30% of the layer's thickness.

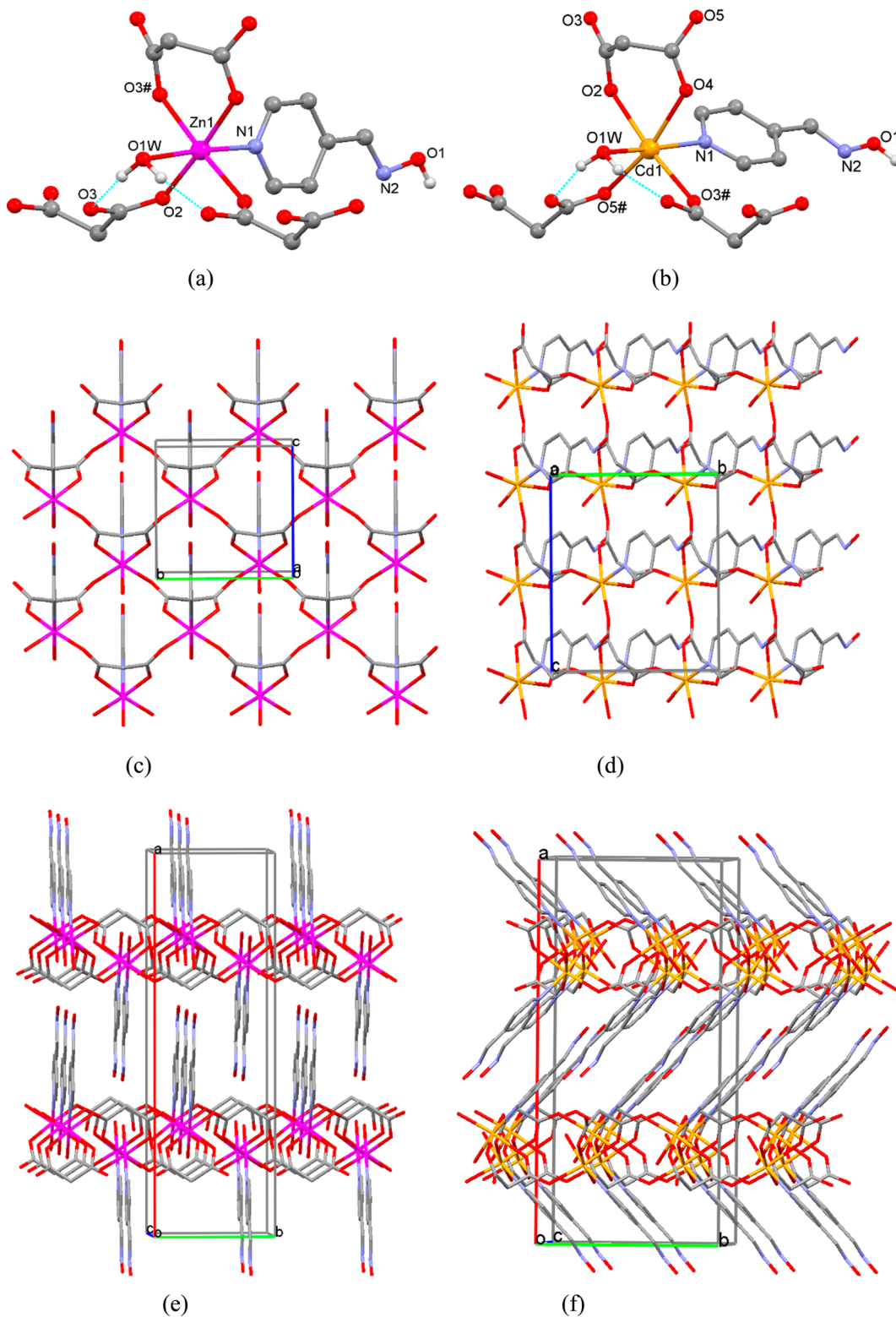


**Figure 4.** (a) View of the MBU in **4** showing the partial atom numbering scheme. Symmetry transformation for symmetry related atoms: #  $-x, -y, -z$ . (b) View of the MBU in **5** showing the partial atom numbering scheme. Symmetry transformations for symmetry related atoms: #  $1/2 - x, y, z + 1/2; 1/2 - x, y - 1/2, z$ . (c) Coordination layer in **4** in projection on the  $bc$  plane. (d) Coordination layer in **5** in projection on the  $bc$  plane. (e) Mode of interpenetration of the layers in **4**. (f) Mode of interpenetration of the layers in **5**.

The interpenetration is reinforced by the OH...O hydrogen bonds with participation of the 4-pyao hydroxyl groups as H-donors and carboxylic oxygen atoms as H-acceptors (Table 2S). No SAVs were found in this structure, and PI is 71.9.

With the use of adipic acid, the supramolecular pseudo isomers<sup>35</sup> 1D polymer  $[\text{Zn}(\text{adi})(\text{4-pyao})_2]_n$  **7**, and 2D polymer  $\{[\text{Cd}(\text{adi})(\text{4-pyao})_2]\cdot\text{dmf}\}_n$  **8** were obtained. Both compounds crystallize in the triclinic centrosymmetric space group  $P\bar{1}$  and

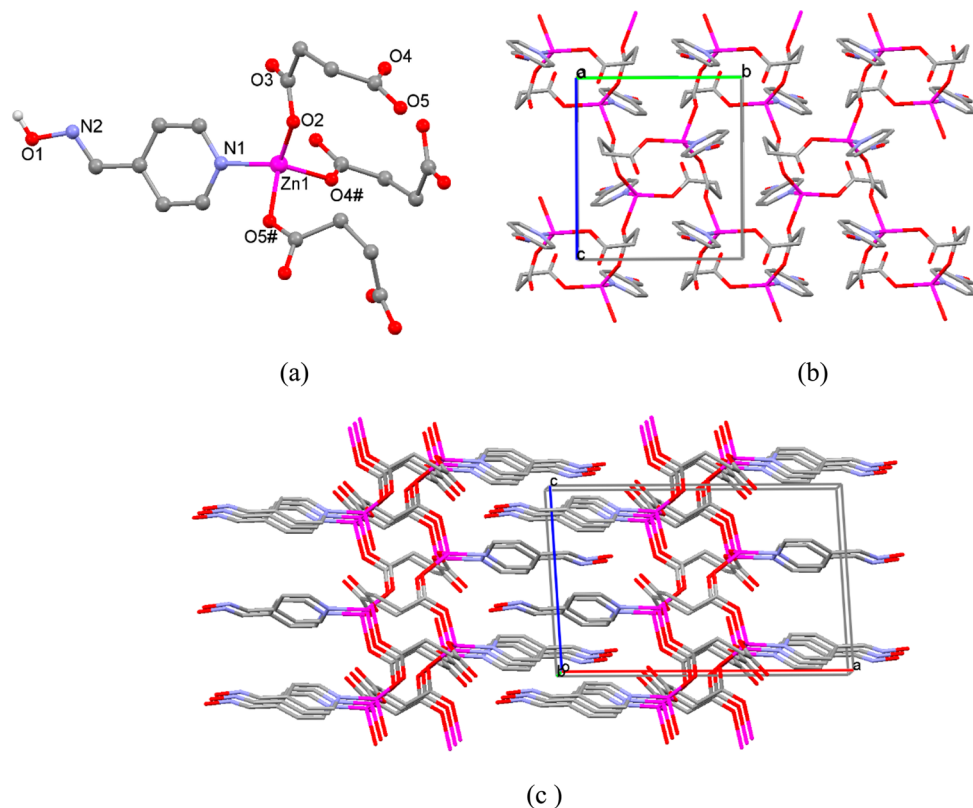


**Figure 5.** (a) View of the MBU in **6** showing the partial numbering scheme. Symmetry transformations for symmetry-related atoms: #  $3/2 - x, y - 1/2, 3/2 - z$ . (b) View of the layer in projection on the  $bc$  plane. (c) Packing of two layers with the interdigitation. C-bound H atoms are omitted for clarity.

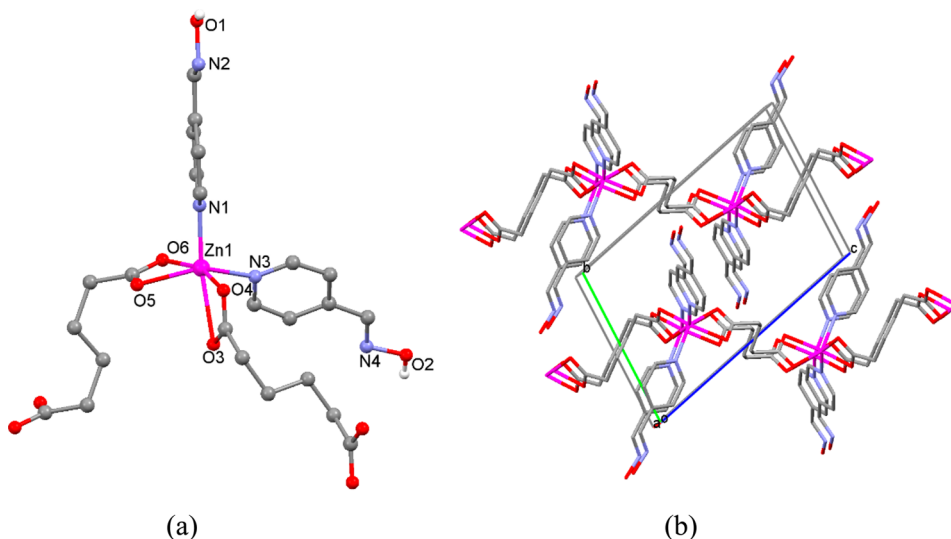


**Figure 6.** (a) Coordination environment of Zn(II) atom in **7** with partial numbering scheme. (b) Packing of polymeric chains. H atoms are omitted.

have the same 1:2 metal/oxime molar ratio. The Zn(II) coordination polyhedron in **7** is shown in Figure 6a. The  $N_2O_4$  octahedron comprises two crystallographically different adipate residues that reside on inversion centers, and two neutral 4-pyao molecules. All carboxylic groups coordinate to the metal in the bidentate chelating modes, the 4-pyao ligands coordinate as usual via pyridine nitrogen atoms. The Zn–O bond distances are in the range 2.029(2)–2.477(2) Å. The Zn–N bond distances are equal to 2.053(2) and 2.084(2) Å (Table 1S). The two 4-pyao ligands display in approximately perpendicular planes, as the dihedral angle of 89.50° between their pyridine rings indicates,

and the two four-membered Zn-carboxylate chelate rings form the dihedral angle of 75.97°. The Zn···Zn separations across the adipate residues in the polymeric chain are equal to 9.53 and 9.94 Å (Figure 6b). The chains are associated in the 3D H-bonded network via oxime OH-groups and carboxylic oxygen atoms (Table 2S). The structure contains negligible (1.1%) SAVs; PI = 67.8.

Compound  $\{[Cd(adi)(4-pyao)] \cdot dmf\}_n$  **8** that differs from **7** by the metal, demonstrates the principally different laminar polymeric framework with the dmf inclusion (Figure 7). The MBU represents the binuclear cluster. Each Cd(II)  $N_2O_5$ -coordination

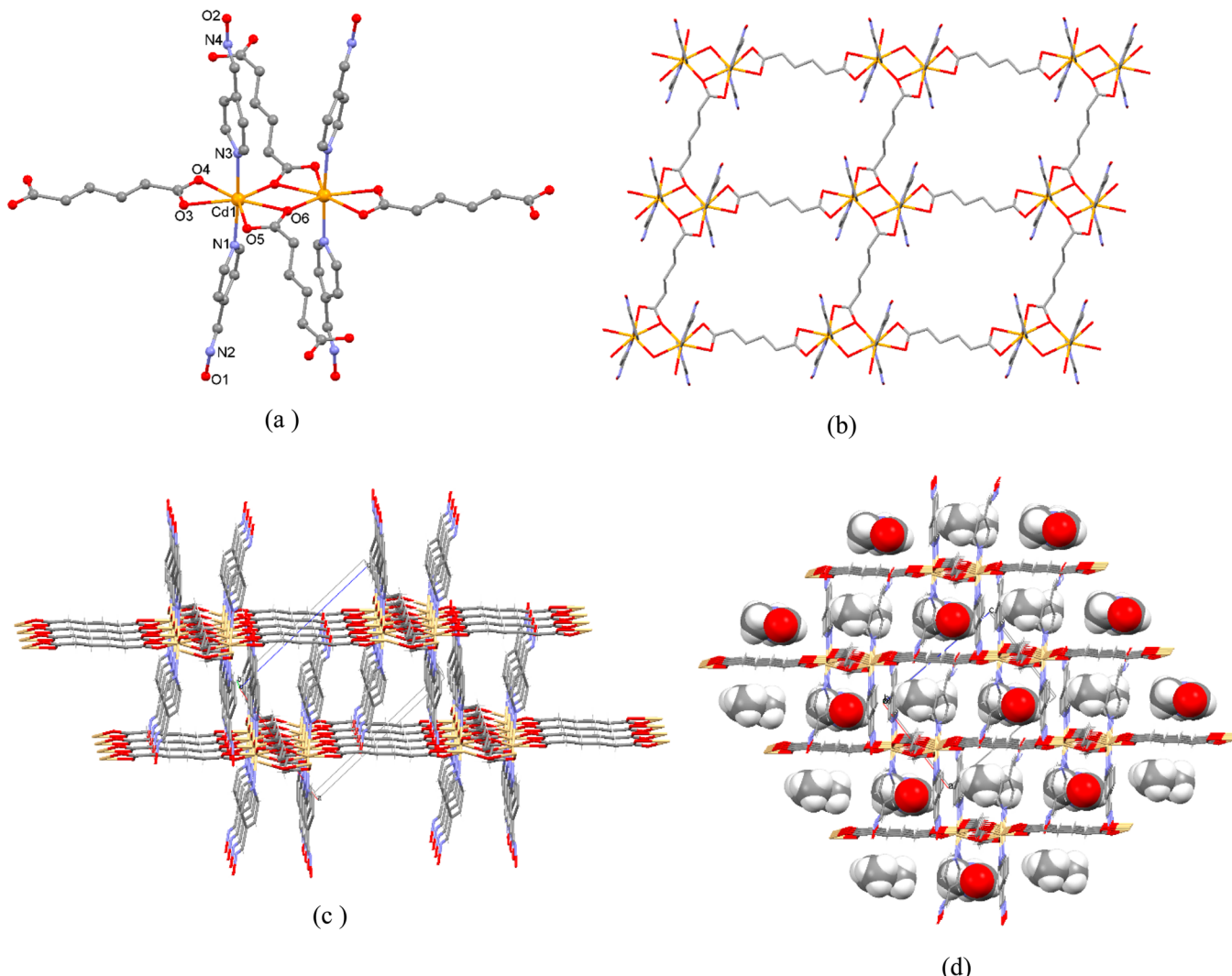


**Figure 7.** (a) View of the MBU in **8** showing the partial numbering scheme. C-bound H atoms are omitted for clarity. (b) Fragment of the layer - top view. (c) The mode of layers' interdigitaion. (d) The dmf inclusion in the crystal lattice. The dmf molecules are shown in the space-filling mode.

core represents the pentagonal bipyramidal that comprises three bidentate-bridging adipate anions in the equatorial plane, and two terminal 4-pyao ligands in the apical positions (Figure 7a). The Cd–O bond distances are within the range 2.308(2)–2.425(2) Å, and the Cd–N bond distances are equal to 2.322(3) Å and 2.328(3) Å (Table 1S). In the centrosymmetric binuclear cluster, the Cd..Cd separation is equal to 3.811 Å (Figure 7a). The extension of these dimeric nodes in two directions through the adipate linkers gives rise to the layer with the (4,4) topology with meshes whose linear dimensions are 11.583 × 11.711 Å measured as the distances between the nearest Cd(II) cations across the adipate anions (Figure 8b). These large meshes provide the deep interdigitation of the pillar 4-pyao molecules from the adjacent layers, which just transect the coordination backbone of the layer. The interdigitation is reinforced by the H-bond interactions with participation of the 4-pyao hydroxyl groups as H-donors and carboxylic oxygen atoms acting as H-acceptors (Table 2S, Figure 7c). The layer thickness is equal 15.549 Å. The depth of interpenetration is 7.871 Å, constituting the 50% of the layer thickness. Thus, the supramolecular architecture rather resembles the 3D MOF than the stacks of H-bonded coordination layers. In spite of the deep interpenetration and self-association of the layers in the 3D H-bonded

network, the dmf molecules are accommodated in the crystal lattice being displayed parallel to the lipophilic fragments of the adipate bridges, and simultaneously in the T-shape mode to the 4-pyao pillars (Figure 7d). It looks like the coordination network is responsive to the positions of the disordered dmf molecules since they correlate with the positions of the disordered 4-pyao pyridine rings. Moreover, this breathing network has 3.9% SAVs calculated with accommodated dmf solvent in the lack of disorder. The SAVs for the solvent-free network give the value of 307 Å<sup>3</sup> (~25% of the unit cell volume) thus indicating the high solvent uptake.

Thus, the 4-pyao ligand being coordinated to the d<sup>10</sup> metals in a monodentate mode affords more opportunities compared with the 2-pyao ligand for the extended coordination networks.

As we mentioned above, our previous findings in using Niox as an auxiliary ligand for construction of coordination networks resulted in the mixed-ligand 1D polymeric arrays that comprise the metal-Niox unit in combination with the monocarboxylate and bpy-type ligands, and 2D solids comprising the metal- Niox unit in combination with sulfate and bpy-type ligands.<sup>49,51</sup> MOMs from the system Zn(II)/Cd(II) - Niox - H<sub>2</sub>adi resulted in supramolecular isomers [Zn(adi)(Niox)]<sub>n</sub> **9** (Figure 8) and [Cd(adi)(Niox)]<sub>n</sub> **10** (Figure 9) that crystallize in the monoclinic

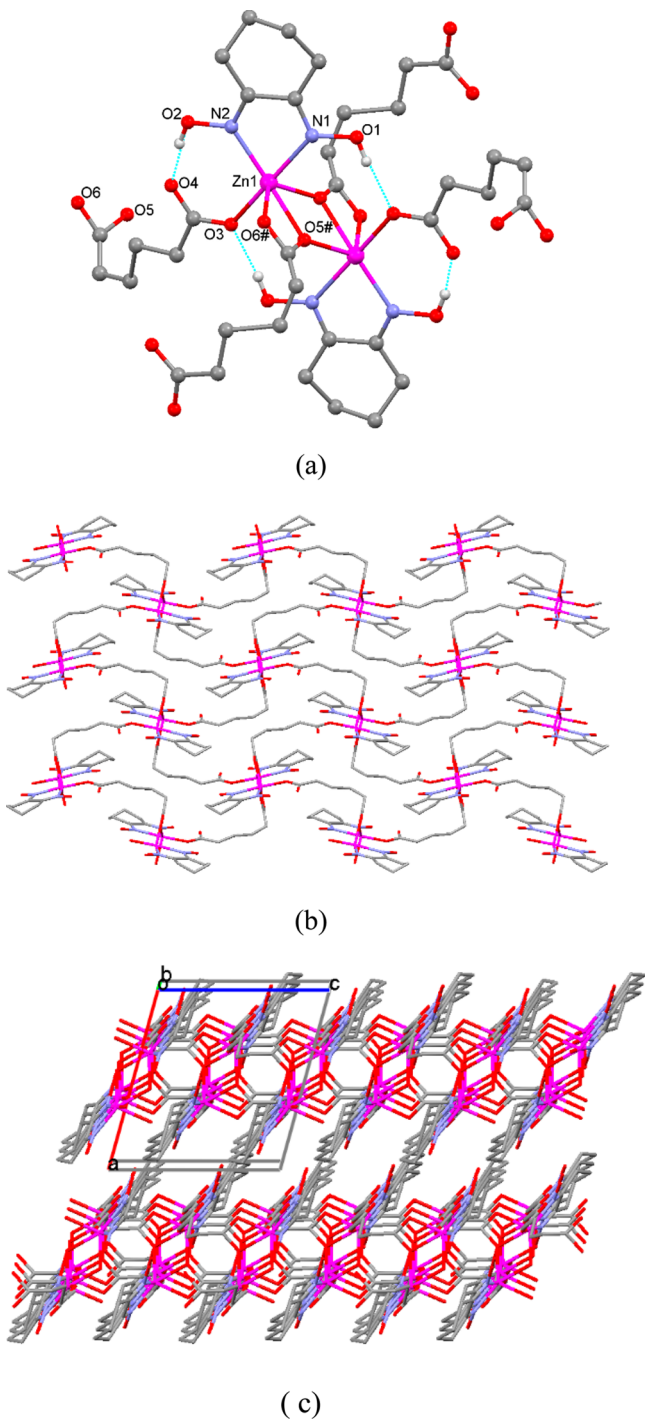


**Figure 8.** (a) View of the binuclear MBU in **9** showing the partial numbering scheme. C-bound H atoms are omitted for clarity. Symmetry transformation for symmetry-related atoms: #  $1-x, -y, -z$ . (b) Fragment of the layer - top view. (c) The mode of layers' stacking.

centrosymmetric space groups  $P2_1/c$  and  $C2/c$ . MOM **9** represents the 2D network, while MOM **10** represents the 3D grid.

The MBU in **9** represents the binuclear cluster built of two Zn(II) octahedra. Each Zn(II) atom adopts the distorted  $N_2O_4$ -octahedral geometry, arising from one Niox ligand coordinated in the  $N,N'$ -chelate mode, and three symmetry-equivalent adipate anions. The Zn–O bond distances are in the range 1.977(8)–2.119(5) Å, and the Zn–N bond distances are equal to 2.091(4) and 2.214(4) Å (Table 1S). The adipate anion acts in the

monodentate and mono, bidentate bridging modes. The self-association of the two Zn(II) octahedra occurs via two inversion-related adipate anions through their mono, bidentate-bridging coordination (Figure 8a). This coordination mode of adipate anion has not been reported in the literature so far (Scheme 1S). The Zn–Zn separation in the binuclear unit across the carboxylato bridge is equal to 3.499 Å. The binuclear metal clusters are associated in a spongy layer with the (4,4) topology being composed of the S-shaped meshes due to the bent conformation of the adipate ligand (Figure 8b). The layers are propagated parallel to the  $bc$  crystallographic plane, and the layer thickness is estimated as 10.696 Å. The layers stack along the crystallographic  $a$  axis and meet by the cyclohexyl rings; the interpenetration is measured as 0.84 Å being minimal among the compounds discussed herein (Figure 8c). This solid similar to **8** demonstrates breathing behavior indicated by the disordering of one of the carboxylate groups that adjust alternatively either bidentate- or monodentate modes of coordination, and by the commonplace disorder of the Niox cyclohexyl ring. The conformational flexibility of the cyclohexane ring in Niox may explain its more effective crystal packing reducing the size of the voids in this crystal solid. Our analysis of the voids in the crystal after the disorder removal yields 111 Å<sup>3</sup> for 0.8 Å probe radius. Furthermore, the adsorption measurements supported by the computations revealed the developed surface acceptable for adsorption. The examples of ultramicroporous materials that otherwise reveal excellent adsorption properties are known from the literature. For example, the so-called “SIFSIX” MOMs reported by Forrest et al.<sup>44</sup> with the narrow pore sizes and small BET surface area, yet exhibit very tight packing of CO<sub>2</sub> in those dense networks. The gas loading correlates with the MOM contraction and pyrazine rings tilting in the structures.<sup>72</sup> Similarly, the availability of the conformationally flexible components in the networks reported by us supports the possible “breathing behavior” and “gate opening” during the adsorption processes.<sup>73</sup>

The 3D MOF **10** with the composition  $[Cd(Niox)(adi)]_n$  crystallizes in the monoclinic  $C2/c$  space group, where each Cd(II) atom resides on the 2-fold axis and adopts distorted  $N_2O_4$ -octahedral geometry, coordinating four adipate anions and one Niox ligand, Cd–O bond distances being 2.371(4) and 2.196(4) Å, and Cd–N bond distance being 2.356(5) Å (Table 1S). The bridging adipate ligands coordinate in a bis-bidentate mode, and the Niox ligand coordinates in a bis-chelate mode (Figure 9a). The network has a (4,4) topology. In the crystallographic  $ac$  plane, the coordination network is built of the rows of eight-membered  $[Cd_2(COO)_2]$  metallocycles with the Cd–Cd separation of 4.926 Å. The rows propagate parallel to the crystallographic  $c$  axis being linked by the bent adipate bridges along the  $a$  axis (Figure 9b). The infinite motif parallel to the crystallographic  $ab$  plane is built of the 36-membered  $[Cd_4(C_6O_2)_4]$  metallocycles with two Niox ligands accommodated within these metallocavities (Figure 9c). Thus, the length and flexibility of adipate anion<sup>74–78</sup> in combination with the larger atomic radius of Cd(II) vs Zn(II) play crucial role in the generation of the 3D structure **10** with the PI 75.8.

**Adsorption Properties for **7** and **9**. The Texture Characteristics of the Samples.** The 1D and 2D polymeric solids **7**, **8** and **9** different in composition and crystal lattice organization were chosen to estimate such important parameters of porous materials as the value of the specific surface area, and the sorption pore volume. The attempt to use sample **8** under conditions identical to **7** and **9** failed because of sample decomposition upon dmso evacuation. Similar to our previous

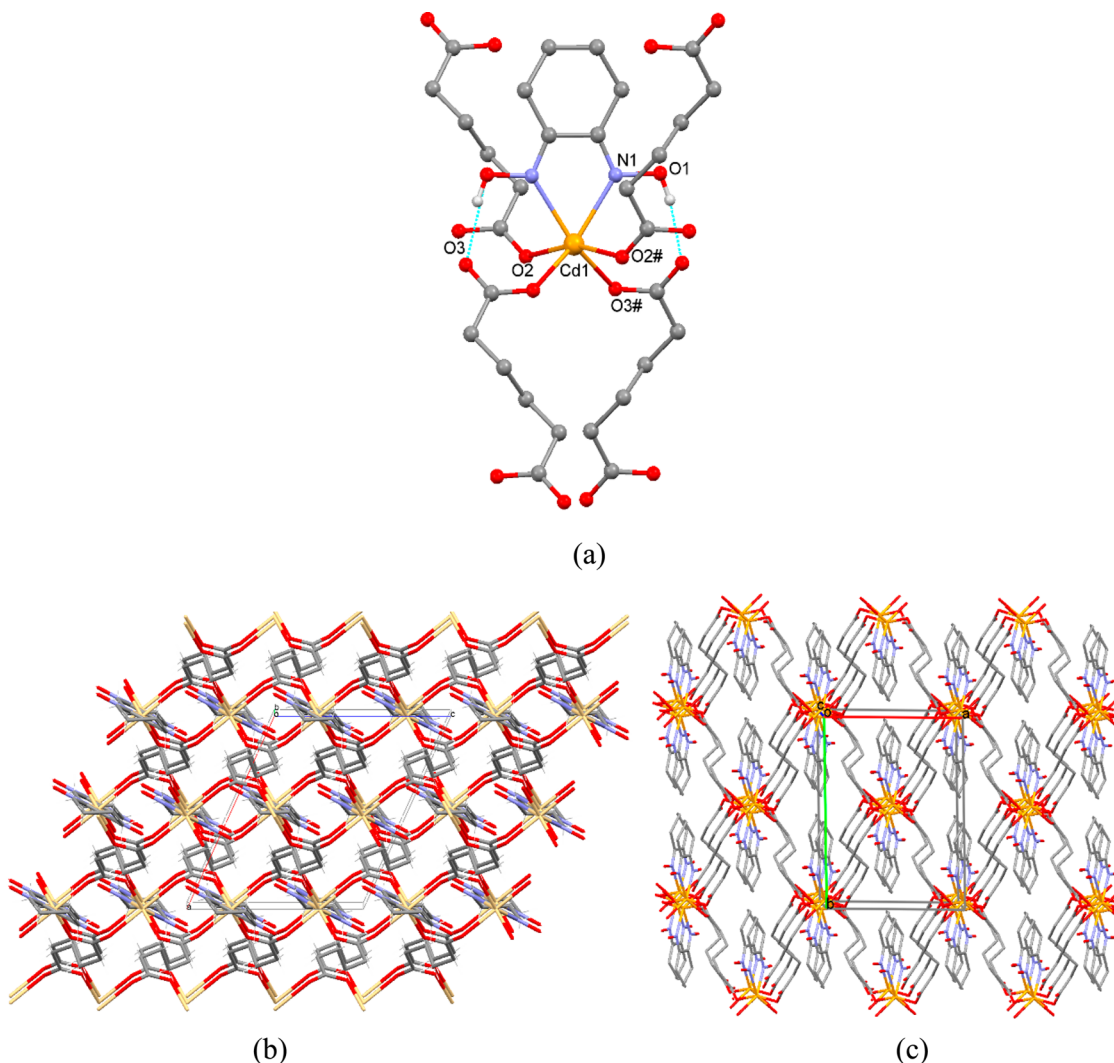


**Figure 9.** (a) View of the MBU in **10** showing the partial atom numbering scheme. Symmetry transformation for symmetry-related atoms: #  $-x, y, \frac{3}{2} - z$ . C-bound H atoms are omitted for clarity. (b) Coordination network in projection on the *ac* plane. (c) Coordination network in projection on the *ab* plane.

investigation,<sup>51</sup> the BET method<sup>79</sup> based on the analysis of low-temperature gas adsorption isotherms has been used to evaluate the texture characteristics of solids **7** and **9** based on the BET equation:

$$a = \frac{a_m K p / p_s}{(1 - p/p_s)[1 + (k - 1)p/p_s]} \quad (1)$$

where  $p/p_s$  is the adsorbate relative pressure,  $a$  is the adsorption value at corresponding  $p/p_s$ ,  $a_m$  is the monolayer capacity, and  $K$  is the BET equation equilibrium constant. To determine the specific surface area of solids by this method, nitrogen is the most often used as an adsorbate at 77 K. Building the isotherms included two stages. In the first stage, the samples were degassed for the removal of traces of moisture and carbon dioxide at 313 K in a vacuum of  $2 \times 10^{-4}$  mm Hg during 1 day, and in the second, the samples were subjected to nitrogen adsorption. The weight of the samples used for the analyses was 0.08 g. The resulting adsorption–desorption isotherms shown in Figure 10 can be attributed to type II isotherm according to BDDT classification.<sup>79</sup>

The isotherm **9** is typical for physical adsorption and indicates the heterogeneous pores in the sample with a predominance of

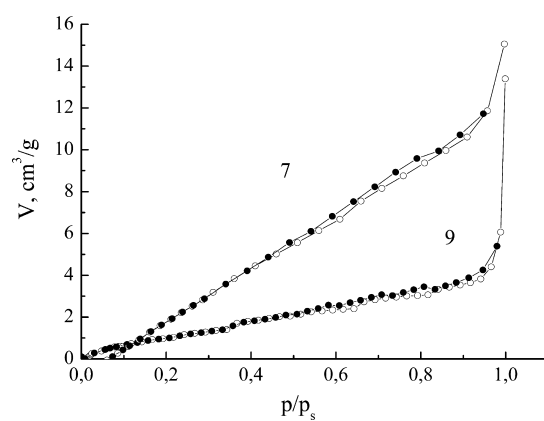


**Figure 10.**  $\text{N}_2$  adsorption (white circles) and desorption (filled circles) isotherms at 77 K for samples **7** and **9**. A small adsorption/desorption hysteresis is observed.

mesopores. The isotherm plot exhibits a slight rise of the curve at the beginning at low relative pressures of nitrogen, a monotonic increase at the relative pressure  $p/p_s$  0.20–0.90 and a sharp rise of the curve after the  $p/p_s > 0.90$ . Initial convex section indicates the

presence of a small amount of micropores; at  $p/p_s = 0.35$  there is an inflection in the isotherm, indicating the completion of the monolayer formation and the beginning of multilayer formation. The isotherm 7 is the same as the isotherm 9, being characteristic for mesopore structure; i.e., the amount of adsorbed substance is proportional to the relative pressure of adsorbate in a large interval of relative pressure. Higher position of isotherm 7 in the plot indicates its more developed pore structure. After the  $p/p_s > 0.90$  in the pores of both samples volumetric filling - capillary condensation of the adsorbate occurs. A small hysteresis observed in the adsorption isotherms indicates that the gas adsorption process is nearly reversible. However, the monocrystalline sample disintegrated into powder at the end of the experiment, indicating destructive nature of the adsorption. The isotherms obtained served as source for determination of main adsorption-structural characteristics of the samples, maximum adsorption capacity, specific area, sorption pore volume, and pore and particles dimensions.

The specific surface area has been calculated as follows:

$$S = a_m N_A \omega_0 \quad (2)$$

where  $N_A$  is Avogadro's number,  $\omega_0$  is the area occupied by one molecule in a dense monolayer, and  $a_m$  is the capacity of a monolayer calculated from linear form of BET equation.<sup>51</sup> For comparison, the specific surface has been also assessed by the monolayer capacity—by the value of the nitrogen adsorption in the isotherm inflection point  $B$  which reflects the filling of the monolayer. Limiting adsorption pore volume  $V_s$  has been calculated as the product of the maximum adsorption of nitrogen ( $a_{\max}$ ) at the relative pressure of nitrogen,  $p/p_s$  equal to 1 on the molar volume of nitrogen in the condensed state ( $V_0$ ):

$$V_s = a_{\max} V_0 \quad (3)$$

Sorption pore volume for sample 7 has been also determined by another independent method, by the adsorption of benzene and dmf vapors in desiccator at saturation. Effective pore diameters were found from the differential curve of pore volumes vs the radii distribution. Pore volumes distribution curves vs the radii (Figure 11) were constructed on the basis of adsorption data and calculated after the BJH method.<sup>80</sup>

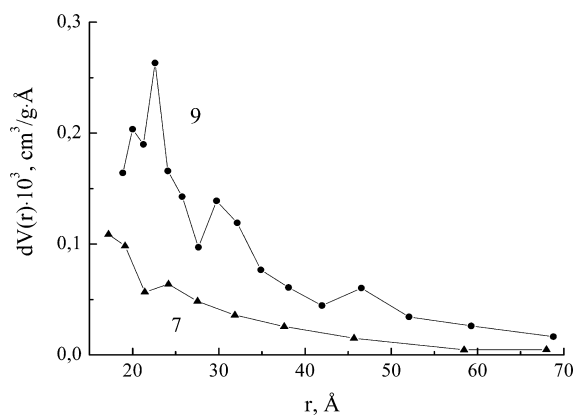


Figure 11. Differential distribution of pore volumes to the radii.

The curves analysis shows that sample 9 has a significant number of pores with the radii of 20–25 Å and the maximum at 22.8 Å. There is observed still two minor peaks with an average pore radius of 30.1 and 46.0 Å in the distribution curve. As for sample 7, there is one small maximum at 24.1 Å in the distribution curve. Effective pore radius  $r_{\text{ef}}$  (Å) has been also calculated

from the experimental data of sorption pore volume and specific surface assuming a cylindrical shape of pores:

$$r_{\text{ef}} = 2V_s/S \quad (4)$$

The particle size  $D$  (nm) has been calculated from the data on the specific surface area ( $S$ , m<sup>2</sup>/g) and the true density ( $\gamma$ , g/cm<sup>3</sup>) as follows:

$$D = 6 \times 10^3 / \gamma S \quad (5)$$

Adsorption and structural characteristics of the samples determined are shown in Table 2. As it can be seen from Table 2, the specific surface area, determined in two ways, shows good agreement, and the relative error does not exceed 5%. The difference in sorption amounts determined after three different adsorbates associated with different sizes of cross-section of the molecules – 16.2, 22.5, and 40 Å<sup>2</sup> for nitrogen, dmf, and benzene, respectively.<sup>81</sup>

Effective pore radius for sample 7 calculated by eq 4 using N<sub>2</sub> shows good agreement with that obtained from the distribution curve (Figure 11), suggesting a cylindrical pore shape. Effective pore radii for sample 9 calculated by the same way using three adsorbates, on the contrary differs considerably from the values evaluated using the distribution curve. This may be related to the noncylindrical shape of pores in the sample. Thus, by the nature of adsorption, effective porosity, and pore size the synthesized samples can be attributed to the sorbents having a nanoporous structure, and molecules with dimensions smaller than the maximum diameter of the pores are in principle free to sorb by the samples.

**Crystal Structure Simulations.** We performed periodical quantum chemical calculations on crystal 9 with and without guest molecules using PM7 Hamiltonian,<sup>82</sup> which includes dispersion correction. Computer program MOPAC2012 was used for all calculations.<sup>83,84</sup> Although periodical DFT, HF, and semi-empirical calculations lack the dispersion component of intermolecular interactions and may result in unbound structures,<sup>85</sup> the empirically added dispersion correction makes both *ab initio* and semiempirical results rather accurate.<sup>82</sup> Another potential source of inaccuracy could be chlorine bonds,<sup>85,86</sup> or other intermolecular interactions with a strong donor–acceptor component.<sup>87,88</sup> Fortunately, neither halogen nor chalcogen atoms are present in the structure 9, making PM7 results reliable in this case.

The initial atomic coordinates for the crystal 9 were taken from the CIF file, with the symmetry reduced to *P1* space group. The crystal structure was optimized first with the lattice parameters frozen, and then relaxed. The resulting formation enthalpy was used to calculate the interaction enthalpy between the crystalline matrix and guest molecule. Mercury software<sup>60</sup> was used to display the voids (0.8 Å probe radius) in the crystal structure. As one can see in Figure 12, the unit cell contains two types of voids, located at the centers of the *a* and *b* edges, each shared between four neighboring unit cells. The combined volume of these voids is close to 111 Å<sup>3</sup>, or 7.7% of the unit cell volume.

The voids of the crystal structure were filled with eight H<sub>2</sub> or N<sub>2</sub> molecules per unit cell. Relaxations of the resulting inclusion structures were distinctly different. While H<sub>2</sub> molecules diffused out of the cavities and did not increase the lattice parameters appreciably (Table 3), the N<sub>2</sub> molecules remained close to the center of the cavities and increased their size so that crystal disintegrated into noninteracting slabs (the parameter *a* increased by more than 1 Å). In order to determine the capacity of the ultramicropores with respect to the number of N<sub>2</sub> molecules, we

Table 2. Adsorption–Structure Characteristics of the Samples 7 and 9<sup>a</sup>

sample	surface area, $S$ , $\text{m}^2/\text{g}$		sorption pore volume, $V_s$ , $\text{cm}^3/\text{g}$			pores effective radius, $r_{\text{eff}}$ , Å	particles size, $D$ , nm
	BET	B point	$\text{N}_2$	DMF	$\text{C}_6\text{H}_6$		
7	21.04	19.40	0.023			21.9	191.2
9	4.99	5.22	0.021	0.0180	0.0135	84.0; 72.1; 54.0	750.0

<sup>a</sup>Note:  $N_A = 6.02 \times 10^{23}$  1/mol;  $\omega_0(\text{N}_2) = 16.2 \text{ \AA}^2$ ;  $V_0(\text{N}_2) = 34.65 \text{ cm}^3/\text{mol}$ .

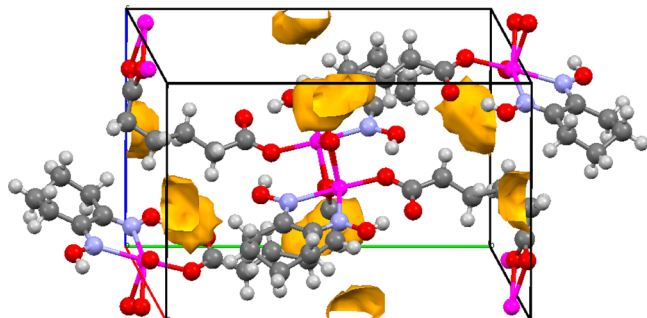


Figure 12. Voids in the simulated crystal 9.

Table 3. Lattice Parameters (Å, °) and Interaction Enthalpies (kcal/mol) for Crystal 9 and Related Inclusion Compounds

system $9*nX$	$a$	$b$	$c$	$\beta$	interaction enthalpy
experiment	10.239	15.342	9.652	105.727	
$n = 0$	10.239	15.342	9.291	105.727	0.00
$n = 8, X = \text{H}_2$	10.645	15.531	9.730	105.122	-0.74
$n = 1, X = \text{N}_2$	10.336	15.660	9.380	104.912	-0.45
$n = 2, X = \text{N}_2$	10.328	15.652	9.364	105.111	-5.63
$n = 3, X = \text{N}_2$	10.587	15.709	9.405	104.746	-5.57
$n = 4, X = \text{N}_2$	11.490	15.671	9.839	104.788	-8.93
$n = 5, X = \text{N}_2$	11.495	15.681	9.875	104.964	-5.85

added one molecule, relaxed the structure, then added another one, etc. The results are listed in Table 3. As one can see, formation of the inclusion complex is energetically favorable in all cases. The addition of the first guest molecule expanded  $b$  by 0.3 Å, so that the interaction energy is largely reduced by the matrix deformation energy. The second molecule enters the matrix that is already expanded, and guest/matrix interaction results in ~5 kcal/mol stabilization. The third molecule expanded  $a$  by extra 0.3 Å, and this deformation again is nearly compensated by the guest/matrix interaction. The fourth and fifth molecules expand  $a$  by extra 0.9 Å and  $c$  by 0.4 Å. Clearly, four  $\text{N}_2$  molecules exceed the capacity of the voids and result in structural disintegration. Formation of the micropores is likely at this stage. This is in agreement with experimental data, described in the previous section. Experimental adsorption data reported in Figure 10 suggest that the interval of relative pressures from 0.1 to 0.95 corresponds to filling of ultramicrocavities in the intact single crystal by 0.1 to 2.8  $\text{N}_2$  molecules per unit cell, while a steep increase at larger relative pressure corresponds to formation of the larger cavities. We also predict that this material is capable of hydrogen storage, as Table 3 reports adsorption of eight  $\text{H}_2$  molecules is energetically favorable and does not result in structural disintegration.

**Photoluminescent Properties.** In continuation of our previous research,<sup>33,48–53</sup> the photoluminescent properties of MOMs 1–10 together with the free oxime ligands were explored at room temperature in the solid state. Compounds were separated in three groups in dependence on the oxime ligand

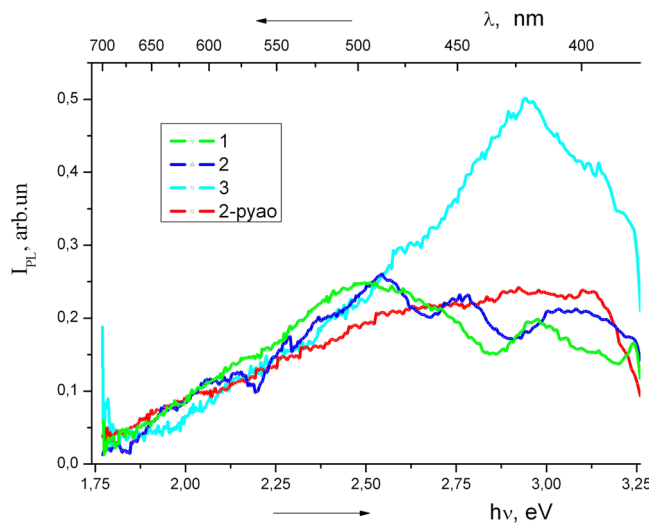


Figure 13. Solid-state luminescence emissions recorded at room temperature for 1–3 and pure 2-pyao.

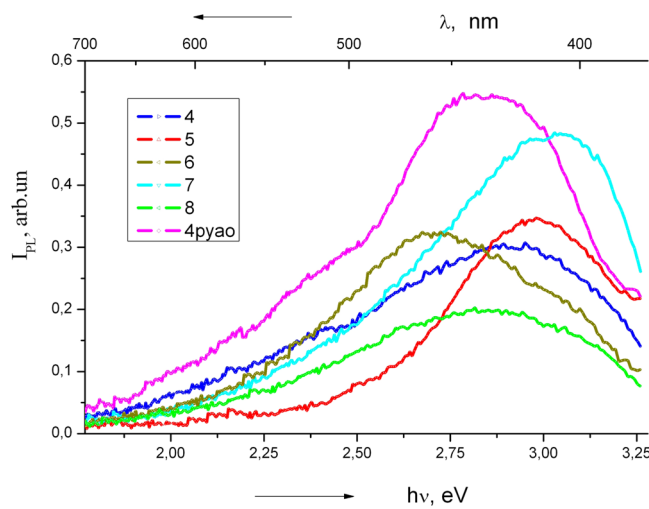
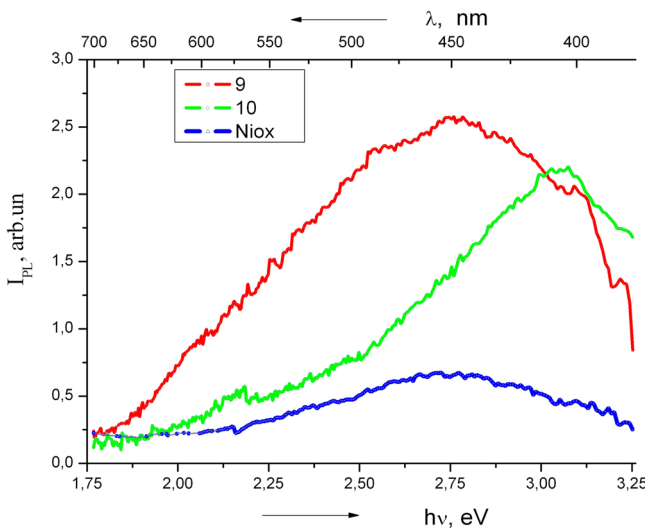


Figure 14. Solid-state luminescence emissions recorded at room temperature for 4–8 and pure 4-pyao.

used, and their emission spectra together with the free ligands were measured and depicted in Figures 13–15. In line with our previous results supported by the quantum-chemical calculations,<sup>53</sup> the emission from these solids can be attributed to the intraligand or ligand-to-ligand charge transfer, specifically to the  $\pi-\pi^*$  or  $n-\pi^*$  transitions. In the first group, the discrete MOMs 1, 2 reveal the rather weak unstructured emission (Figure 13). The 1D polymeric solid 3 demonstrates an essential increase in the emission intensity compared with 1, 2, and pure 2-pyao, that can be assigned to the two concerted events, the lack of the guests that usually quench the emission, and the more effective crystal packing (Figure 3) with parallel arrangement and overlapping of the 2-pyao aromatic units. The rather unusual result was



**Figure 15.** Solid-state luminescence emissions recorded at room temperature for **9**, **10**, and pure Niox.

observed for **4–8** containing 4-pyao. As it follows from the plot (Figure 14), all materials demonstrate essentially lower emission intensity compared with the pure 4-pyao. The reasons for the emission quenching in this group may originate from (a) the low relative content of 4-pyao in the polymeric materials **4–6** with the metal: 4-pyao molar ratio 1:1; (b) the insufficient crystal packing efficacy in the same solids provided by the terminal pillared 4-pyao ligands; (c) the incorporation of dmf as a guest in the crystal lattice **8** suppressing the emission similarly to the previously reported by us the dmf-containing samples.<sup>49</sup> Only the guest-free 1D polymer **7** with the metal: 4-pyao molar ratio 1:2 demonstrates the emission comparable in intensity with the 4-pyao. In the third group both 2D and 3D polymeric materials **9** and **10** emit more strongly than the Niox ligand itself (Figure 15).

## CONCLUSIONS

The dicarboxylic acid/oxime blend approach<sup>46,47</sup> proved its efficacy for fabrication of 10 new MOMs with cumulative properties. Pyridine-2-aldoxime (2-pyao), pyridine-4-aldoxime (4-pyao), and 1,2-cyclohexanedionedioxime (Niox) act as terminal ligands providing an access to the 1D, 2D, and 3D structures where aliphatic dicarboxylates act as the multidentate linkers. The rotatable 4-pyao and flexible Niox ligands afford the extended surface areas due to the deep interpenetration of the former and the perfect accommodation of the latter within the 2D and 3D crystal solids. The selected samples demonstrate an efficient water and dmf uptake explained by the availability of the hydrophilic and hydrophobic regions in these solids. The crystal structure simulations undertaken for one laminar sample and supported by the adsorption measurements reveal their efficacy for the prediction of the adsorption capacity of the solids even in the absence of the registered solvent-accessible voids.<sup>39,89</sup> All materials demonstrate blue-green emission in the solid state.

## ASSOCIATED CONTENT

### Supporting Information

Synthetic procedures, additional figures, tables with the selected bond distances, angles and H-bonds, as well as the X-ray crystallographic files in CIF format. This material is available free of charge via the Internet at <http://pubs.acs.org>. Crystallographic

data for new structures reported herein were deposited with the Cambridge Crystallographic Data Centre and allocated the deposition numbers CCDC 1008081–1008091. These data can be obtained free of charge from the Cambridge Crystallographic Data Centre via [www.ccdc.cam.ac.uk/data\\_request/cif](http://www.ccdc.cam.ac.uk/data_request/cif)

## AUTHOR INFORMATION

### Corresponding Author

\*E-mail: fonari.xray@phys.asm.md, fonari.xray@gmail.com. Tel: +373 22 73 81 54. Fax: +373 22 73 81 49.

### Notes

The authors declare no competing financial interest.

## ACKNOWLEDGMENTS

The authors from Chisinau acknowledge the financial support from the State Program of R. Moldova (Project 14.518.02.04A). This work was supported in part by the U.S. National Science Foundation (CHE-0832622). H.J.R.J. and A.E.M. acknowledge the use of computational resources at The Stokes Advanced Research Computing Center, University of Central Florida (UCF).

## REFERENCES

- (1) Yaghi, O. M.; Davis, C. E.; Li, G.; Li, H. *J. Am. Chem. Soc.* **1997**, *119*, 2861.
- (2) Li, H.; Davis, C. E.; Groy, T. L.; Kelley, D. G.; Yaghi, O. M. *J. Am. Chem. Soc.* **1998**, *120*, 2186.
- (3) Li, H.; Eddaoudi, M.; Groy, T. L.; Yaghi, O. M. *J. Am. Chem. Soc.* **1998**, *120*, 8571.
- (4) Eddaoudi, M.; Li, H.; Reineke, T.; Fehr, M.; Kelley, D.; Groy, T. L.; Yaghi, O. M. *Top. Catal.* **1999**, *9*, 105.
- (5) Eddaoudi, M.; Li, H.; Yaghi, O. M. *J. Am. Chem. Soc.* **2000**, *122*, 1391.
- (6) Eddaoudi, M.; Moler, D. B.; Li, H.; Chen, B.; Reineke, T. M.; O'Keeffe, M.; Yaghi, O. M. *Acc. Chem. Res.* **2001**, *34*, 319.
- (7) Pan, L.; Sander, M. B.; Huang, X.; Li, J.; Smith, M.; Bittner, E.; Bockrath, B.; Johnson, J. K. *J. Am. Chem. Soc.* **2004**, *126*, 1308.
- (8) Perry, J. J.; Perman, J. A.; Zaworotko, M. J. *Chem. Soc. Rev.* **2009**, *38*, 1400.
- (9) Husain, A.; Ellwart, M.; Bourne, S. A.; Öhrström, L.; Oliver, C. L. *Cryst. Growth Des.* **2013**, *13*, 1526.
- (10) Fang, Q.; Zhu, G.; Xue, M.; Sun, J.; Sun, F.; Qiu, S. *Inorg. Chem.* **2006**, *45*, 3582.
- (11) Manos, M. J.; Moushi, E. E.; Papaefstathiou, G. S.; Tasiopoulos, A. *J. Cryst. Growth Des.* **2012**, *12*, 5471.
- (12) Yang, W.; Lin, X.; Blake, A. J.; Wilson, C.; Hubberstey, P.; Champness, N. R.; Schröder, M. *Inorg. Chem.* **2009**, *48*, 11067.
- (13) Lee, J. Y.; Fahra, O. K.; Roberts, J.; Scheidt, K. A.; Nguyen, S. B. T.; Hupp, J. T. *Chem. Soc. Rev.* **2009**, *38*, 1450.
- (14) Corma, A.; García, H.; Llabrés i Xamena, F. X. *Chem. Rev.* **2010**, *110*, 4606.
- (15) Meng, W.; Xu, Z.; Ding, J.; Wu, D.; Han, X.; Hou, H.; Fan, Y. *Cryst. Growth Des.* **2014**, *14*, 730.
- (16) Shin, J. W.; Bae, J. M.; Kim, C.; Min, K. S. *Inorg. Chem.* **2013**, *52*, 2265.
- (17) Kan, W.-Q.; Liu, B.; Yang, J.; Liu, Y.-Y.; Ma, J.-F. *Cryst. Growth Des.* **2012**, *12*, 2288.
- (18) Dai, M.; Su, X.-R.; Wang, X.; Wu, B.; Ren, Z.-G.; Zhou, X.; Lang, J.-P. *Cryst. Growth Des.* **2014**, *14*, 240.
- (19) Kreno, L. E.; Leong, K.; Farha, O. K.; Allendorf, M.; Van Duyne, R. P.; Hupp, J. P. *Chem. Rev.* **2012**, *112*, 1105.
- (20) Chen, D.-S.; Sun, L.-B.; Liang, Z.-Q.; Shao, K.-Z.; Wang, C.-G.; Su, Z.-M.; Xing, H.-Z. *Cryst. Growth Des.* **2013**, *13*, 4092.
- (21) Guo, H.-D.; Guo, X.-M.; Batten, S. R.; Song, J.-F.; Song, S.-Y.; Dang, S.; Zheng, G.-L.; Tang, J.-K.; Zhang, H.-J. *Cryst. Growth Des.* **2009**, *9*, 1394.

- (22) Wang, X.; Qin, C.; Wang, E.; Li, Y.; Hao, N.; Hu, C.; Xu, L. *Inorg. Chem.* **2004**, *43*, 1850.
- (23) Zhang, X.; Hou, L.; Liu, B.; Cui, L.; Wang, Y.-Y.; Wu, B. *Cryst. Growth Des.* **2013**, *13*, 3177.
- (24) Evans, O. R.; Lin, W. *Acc. Chem. Res.* **2002**, *35*, 511.
- (25) Lin, W.; Wang, Z.; Ma, L. *J. Am. Chem. Soc.* **1999**, *121*, 11249.
- (26) Zang, S.; Su, Y.; Li, Y.; Ni, Z.; Meng, Q. *Inorg. Chem.* **2006**, *45*, 174.
- (27) Yu, J.; Cui, Y.; Xu, H.; Yang, Y.; Wang, Z.; Chen, B.; Qian, G. *Nat. Commun.* **2013**, *4*, No. 2719.
- (28) Nie, C.; Zhang, Q.; Ding, H.; Huang, B.; Wang, X.; Zhao, X.; Li, S.; Zhou, H.; Wu, J.; Tian, Y. *Dalton Trans.* **2014**, *43*, 599.
- (29) Xu, D.; Yang, M.; Wang, Y.; Cao, Y.; Fang, M.; Zhu, W.; Zhou, H.; Hao, F.; Wu, J.; Tian, Y. *J. Coord. Chem.* **2013**, *66*, 2992.
- (30) Hu, H.; Fishman, D. A.; Gerasov, A. O.; Przhonska, O. V.; Webster, S.; Padilha, L. A.; Peceli, D.; Shandura, M.; Kovtun, Yu. P.; Kachkovski, A. D.; Nayyar, I. H.; Masunov, A. E.; Tongwa, P.; Timofeeva, T. V.; Hagan, D. J.; Van Stryland, E. W. *J. Phys. Lett.* **2012**, *3*, 1222.
- (31) Suponitsky, K. Yu; Masunov, A. E. *J. Chem. Phys.* **2013**, *139*, No. 094310.
- (32) Draguta, S.; Fonari, M. S.; Masunov, A. E.; Antipin, M. Yu.; Timofeeva, T. V. *CrystEngComm* **2013**, *15*, 4700.
- (33) Croitor, L.; Coropceanu, E. B.; Masunov, A. E.; Rivera-Jacquez, H. J.; Siminel, A. V.; Fonari, M. S. *J. Phys. Chem. C* **2014**, *118*, 9217.
- (34) Nayyar, I. H.; Masunov, A. E.; Tretiak, S. *J. Phys. Chem. C* **2013**, *117*, 18170.
- (35) Moulton, B.; Zaworotko, M. *J. Chem. Rev.* **2001**, *101*, 1629.
- (36) Tian, Z.; Lin, J.; Su, Y.; Wen, L.; Liu, Y.; Zhu, H.; Meng, Q.-J. *Cryst. Growth Des.* **2007**, *7*, 1863.
- (37) Tan, Y. S.; Sudlow, A. L.; Molloy, K. C.; Morishima, Y.; Fujisawa, K.; Jackson, W. J.; Henderson, W.; Halim, S. N. B. A.; Ng, S. W.; Tieckink, E. R. T. *Cryst. Growth Des.* **2013**, *13*, 3046.
- (38) Chen, D.-S.; Sun, L.-B.; Liang, Z.-Q.; Shao, K.-Z.; Wang, C.-G.; Su, Z.-M.; Xing, H.-Z. *Cryst. Growth Des.* **2013**, *13*, 4092.
- (39) Mukherjee, G.; Biradha, K. *Chem. Commun.* **2014**, *50*, 670.
- (40) Furukawa, H.; Gándara, F.; Zhang, Y.-B.; Jiang, J.; Queen, W. L.; Hudson, M. R.; Yaghi, O. M. *J. Am. Chem. Soc.* **2014**, *136*, 4369.
- (41) Luebke, R.; Weseliński, L. J.; Belmabkhout, Y.; Chen, Z.; Wojtas, L.; Eddaoudi, M. *Cryst. Growth Des.* **2014**, *14*, 414.
- (42) Flage-Larsen, E.; Thorshaug, K. *Inorg. Chem.* **2014**, *53*, 2569.
- (43) Pham, T.; Forrest, K. A.; Nugent, P.; Belmabkhout, Y.; Luebke, R.; Eddaoudi, M.; Zaworotko, M. J.; Space, B. *J. Phys. Chem. C* **2013**, *117*, 9340.
- (44) Forrest, K. A.; Pham, T.; Hogan, A.; McLaughlin, K.; Tudor, B.; Nugent, P.; Burd, S. D.; Mullen, A.; Cioce, C. R.; Wojtas, L.; Zaworotko, M. J.; Space, B. *J. Phys. Chem. C* **2013**, *117*, 17687.
- (45) Sarkisov, L.; Martin, R. L.; Haranczyk, M.; Smit, B. *J. Am. Chem. Soc.* **2014**, *136*, 2228.
- (46) Papaefstathiou, G. S.; Escuer, A.; Mautner, F. A.; Raptopoulou, C.; Terzis, A.; Perlepes, S. P.; Vicente, R. *Eur. J. Inorg. Chem.* **2005**, 879.
- (47) Stamatatos, T. C.; Diamantopoulou, E.; Raptopoulou, C. P.; Psycharis, V.; Escuer, A.; Perlepes, S. P. *Inorg. Chem.* **2007**, *46*, 2350.
- (48) Croitor, L.; Coropceanu, E. B.; Jeanneau, E.; Dementiev, I. V.; Goglidze, T. I.; Chumakov, Y. M.; Fonari, M. S. *Cryst. Growth Des.* **2009**, *9*, 5233.
- (49) Croitor, L.; Coropceanu, E. B.; Siminel, A. V.; Kravtsov, V. Ch.; Fonari, M. S. *Cryst. Growth Des.* **2011**, *11*, 3536.
- (50) Croitor, L.; Coropceanu, E. B.; Siminel, A. V.; Botoshansky, M. M.; Fonari, M. S. *Inorg. Chim. Acta* **2011**, *370*, 411.
- (51) Croitor, L.; Coropceanu, E. B.; Siminel, A. V.; Kulikova, O.; Zelentsov, V. I.; Datsko, T.; Fonari, M. S. *CrystEngComm.* **2012**, *14*, 3750.
- (52) Coropceanu, E. B.; Croitor, L.; Fonari, M. S. *Polyhedron* **2012**, *38*, 68.
- (53) Croitor, L.; Coropceanu, E. B.; Siminel, A. V.; Masunov, A. E.; Fonari, M. S. *Polyhedron* **2013**, *60*, 140.
- (54) Wen, G.-L.; Wang, Y.-Y.; Zhang, W.-H.; Ren, C.; Liu, R.-T.; Shi, Q.-Z. *CrystEngComm* **2010**, *12*, 1238.
- (55) Mao, H.; Zhang, C.; Li, G.; Zhang, H.; Hou, H.; Li, L.; Wu, Q.; Zhu, Y.; Wang, E. *Dalton Trans.* **2004**, 3918.
- (56) Dey, B.; Das, A.; Choudhury, S. R.; Jana, A. D.; Lu, L.-P.; Zhu, M.-L.; Mukhopadhyay, S. *Inorg. Chim. Acta* **2010**, *363*, 981.
- (57) Du, M.; Jiang, X.-J.; Zhao, X.-J. *Inorg. Chem. Commun.* **2006**, *9*, 1199.
- (58) Cadmium salts are carcinogenic and toxic: (a) *Cadmium in the Environment and Its Significance to Man* (Pollution paper No. 17); Her Majesty's Stationery Office: London, 1980. (b) Lewis, R. J. *Sax's Dangerous Properties of Industrial Materials*. 9th ed. Volumes 1-3. New York, NY: Van Nostrand Reinhold, 1996.
- (59) Sheldrick, G. M. *Acta Crystallogr.* **2008**, *A64*, 112.
- (60) Macrae, C. F.; Edgington, P. R.; McCabe, P.; Pidcock, E.; Shields, G. P.; Taylor, R.; Towler, M.; van de Streek, J. *J. Appl. Crystallogr.* **2006**, *39*, 453.
- (61) Spek, A. L. *J. Appl. Crystallogr.* **2003**, *36*, 7.
- (62) Max, J.-J.; Chapados, C. *J. Phys. Chem. A* **2004**, *108*, 3324.
- (63) Burrows, A. D.; Donovan, A. S.; Harrington, R. W.; Mahon, M. F. *Eur. J. Inorg. Chem.* **2004**, 4686.
- (64) Ang, S. G.; Sun, B. W. *Cryst. Growth Des.* **2005**, *5*, 383.
- (65) Xu, C.; Guo, Q.; Wang, X.; Hou, H.; Fan, Y. *Cryst. Growth Des.* **2011**, *11*, 1869.
- (66) Martin, D. P.; Supkowski, R. M.; LaDuca, R. *Dalton Trans.* **2009**, *514*.
- (67) Caballero, A. B.; Rodriguez-Dieguex, A.; Lezama, L.; Salas, J. M. *Cryst. Growth Des.* **2012**, *12*, 3583.
- (68) Bowden, T. A.; Milton, H. L.; Slawin, A. M. Z.; Lightfoot, P. *Dalton Trans.* **2003**, 936.
- (69) Cui, F.-Y.; Huang, K.-L.; Xu, Y.-Q.; Han, Z.-G.; Liu, X.; Chi, Y.-N.; Hu, C.-W. *CrystEngComm* **2009**, *11*, 2757.
- (70) Lloyd, G. O.; Atwood, J. L.; Barbour, L. *J. Chem. Commun.* **2005**, 1845.
- (71) Nassimbeni, L. *R. Acc. Chem. Res.* **2003**, *36*, 631.
- (72) Nugent, P.; Belmabkhout, Y.; Burd, S. D.; Cairns, A. J.; Luebke, R.; Forrest, K.; Pham, T.; Ma, S.; Space, B.; Wojtas, L.; Eddaoudi, M.; Zaworotko, M. *J. Nature* **2013**, 495, 80.
- (73) Alhamami, M.; Doan, H.; Cheng, C.-H. *Materials* **2014**, *7*, 3198.
- (74) Wilson, J. A.; Uebler, J. W.; LaDuca, R. L. *CrystEngComm* **2013**, *15*, 5218.
- (75) Klaus, S.; Lehenmeier, M. W.; Herdtweck, E.; Deglmann, P.; Ott, A. K.; Rieger, B. *J. Am. Chem. Soc.* **2011**, *133*, 13151.
- (76) Jiang, H.; Ma, J.-F.; Zhang, W.-L.; Liu, Y.-Y.; Yang, J.; Ping, G.-J.; Su, Z.-M. *Eur. J. Inorg. Chem.* **2008**, 745.
- (77) Sadakiyo, M.; Yamada, T.; Kitagawa, H. *J. Am. Chem. Soc.* **2009**, *131*, 9906.
- (78) Cheng, L.; Lin, J.-B.; Gong, J.-Z.; Sun, A.-P.; Ye, B.-H.; Chen, X.-M. *Cryst. Growth Des.* **2006**, *6*, 2739.
- (79) Brunauer, S.; Emmett, P. H.; Teller, E. *J. Am. Chem. Soc.* **1940**, *62*, 1723.
- (80) Barrett, E. P.; Joyner, L. G.; Halenda, P. P. *J. Am. Chem. Soc.* **1951**, *73*, 373.
- (81) Gregg, S. J.; Sing, K. S. W. *Adsorption, Surface Area, and Porosity*, 2nd ed.; Academic Press: New York, 1967.
- (82) Stewart, J. J. P. *J. Mol. Mod.* **2013**, *1* (32), 19.
- (83) Stewart, J. J. P. MOPAC2012, Stewart Computational Chemistry Version 14.083L; Web: <http://OpenMOPAC.net>.
- (84) Maia, J. D. C.; Urquiza Carvalho, G. A.; Mangueira, C. P.; Santana, S. R.; Cabral, L. A. F.; Rocha, G. B. *J. Chem. Theory Comput.* **2012**, *8*, 3072.
- (85) Cardenas-Jiron, G. I.; Masunov, A.; Dannenberg, J. J. *J. Phys. Chem. A* **1999**, *103*, 7042.
- (86) Masunov, A. E.; Zorkii, P. M. *Russ. J. Phys. Chem.* **1992**, *66*, 31.
- (87) Vyboishchikov, S. F.; Masunov, A. E.; Streletsov, V. A.; Tsirel'son, V. G. *Russ. J. Phys. Chem.* **1994**, *68*, 1837.
- (88) Masunov, A. E.; Zorkii, P. M. *J. Struct. Chem.* **1992**, *33*, 423.
- (89) Seo, J.; Matsuda, R.; Sakamoto, H.; Bonneau, C.; Kitagawa, S. *J. Am. Chem. Soc.* **2009**, *131*, 12792.